Nanoelectronics and Its New Materials – A NEW ERA OF NANOSCIENCE

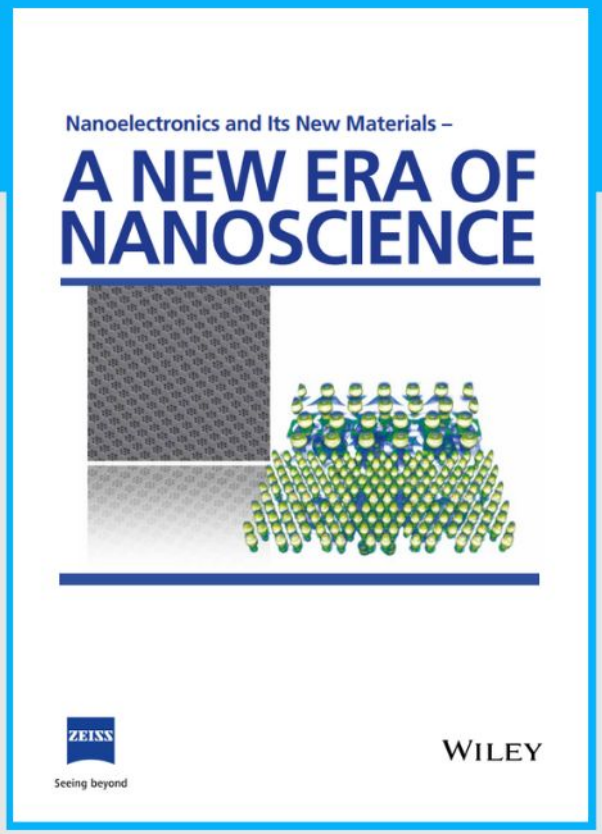

Discover the recent advances in electronics research and fundamental nanoscience.

Nanotechnology has become the driving force behind breakthroughs in engineering, materials science, physics, chemistry, and biological sciences. In this compendium, we delve into a wide range of novel applications that highlight recent advances in electronics research and fundamental nanoscience. From surface analysis and defect detection to tailored optical functionality and transparent nanowire electrodes, this eBook covers key topics that will revolutionize the future of electronics.

To get your hands on this valuable resource and unleash the power of nanotechnology, simply download the eBook now. Stay ahead of the curve and embrace the future of electronics with nanoscience as your guide.

ZEISS

Seeing beyond

WILEY

ADVANCED FUNCTIONAL MATERIALS
www.afm-journal.de

Strain-Insensitive Self-Powered Tactile Sensor Arrays Based on Intrinsically Stretchable and Patternable Ultrathin Conformal Wrinkled Graphene-Elastomer Composite

Jiang He, Runhui Zhou, Yufei Zhang, Wenchao Gao, Tao Chen,* Wenjie Mai,* and Caofeng Pan**

Tissue-like intrinsically stretchable electronics have attracted ever-increasing study attention in recent years as they can form intimate interfaces with skin, endowing devices monitoring tactile and physiological signals with the negligibly constraining movement of the human body. However, harsh mechanical deformation inevitably leads to degradation of or even destroys the electronic properties of the devices. Strain-insensitive self-powered triboelectric tactile sensor arrays based on wafer-scale patterned and intrinsically stretchable nanoscale thin conformal wrinkled graphene-elastomer composite material are demonstrated here. By regulating the wrinkle structure of the composite, the stretchability performance of the material can be optimized. The fabrication process of the composite can be readily incorporated into photolithography and shadow mask techniques without high temperature, annealing, etching, or organic solvents operating. An intrinsically stretchable semitransparent pressure sensor array is created, which can be stretched to 100% strain without visible signals output degradation. The theoretical modeling points out that the unique conformal wrinkle structure is the key element that attributes to the strain-insensitive property of the device. This work offers an alternative approach for the design of novel graphene-based strain-insensitive stretchable soft electronic devices.

1. Introduction

The soft skin-like flexible and stretchable wearable devices are underpinning the development of future biointegrated systems, noninvasive health monitoring, and soft robotics technologies. In this regard, the development of flexible/stretchable materials and devices has attracted ever-increasing study attention in recent years.[1,2] Various flexible sensors and transistors, stretchable electrodes and circuits, and E-skins have been continuously developed.[3] In various application conditions, flexible electronics must stick to and deform with the curved skin surface, thus the device should have good stability,[4] biocompatibility, breathable,[5] self-healable,[6] superior flexibility, and stretchability.[7–10] Therefore, the electrodes in devices could wear on the skin comfortably for a long time and provide stable electrical properties under various harsh mechanical deformations.[7] However, developing and engineering intrinsically

J. He, W. Mai
Siyuan Laboratory
Guangdong Provincial Engineering Technology Research Center of Vacuum Coating Technologies and New Energy Materials
Department of Physics
Jinan University
Guangzhou, Guangdong 510632, China
E-mail: wenjiemai@email.jnu.edu.cn

J. He, R. Zhou, Y. Zhang, C. Pan
CAS Center for Excellence in Nanoscience
Beijing Key Laboratory of Micro-Nano Energy and Sensor
Beijing Institute of Nanoenergy and Nanosystems
Chinese Academy of Sciences
Beijing 101400, P. R. China
E-mail: cfpan@binn.cas.cn

The ORCID identification number(s) for the author(s) of this article can be found under https://doi.org/10.1002/adfm.202107281.

R. Zhou, Y. Zhang, T. Chen, C. Pan
School of Nanoscience and Technology
University of Chinese Academy of Sciences
Beijing 100049, China
E-mail: tao.chen@nimte.ac.cn

W. Gao
Department of Civil Engineering
Monash University
Clayton 3800, Australia
E-mail: wenchao.gao1@monash.edu

T. Chen
Key Laboratory of Marine Materials and Related Technologies
Zhejiang Key Laboratory of Marine Materials and Protective Technologies
Ningbo Institute of Materials Technology and Engineering
Chinese Academy of Sciences
Ningbo 315201, China

DOI: 10.1002/adfm.202107281

stretchable electronic material and the device remains a great challenge.[8,11] In recent years, a new type of self-powered flexible device based on triboelectric nanogenerator has been intensively investigated for its vast application potential in various fields, including implantable medical systems,[12] robot, human–machine interaction,[9] health monitoring,[13] biomimetics, etc. Especially, the fast advances in flexible and wearable energy harvesting technologies are now promoting this research field to the new frontiers.[14] Thus, developing novel flexible and stretchable materials with high-performance, good biocompatible, and low-cost fabrication processes for self-powered electronics are highly sought.

Graphene is an ideally suited material for exploring conceptually novel flexible wearable devices due to its highly desirable properties, including stability, flexibility and durability, high transparency, high conductivity, and good biocompatibility.[15] Owing to the above fascinating properties, graphene has been long considered to have high potential applications in the fabrication of wearable flexible devices.[2,16] Despite the advantages of graphene, the implementation of highly integrated and intrinsically stretchable graphene-based soft devices has been long confined by several issues, especially two main challenges: First, the 2D honeycomb-like carbon-carbon network structure cannot provide sufficient energy dissipation mechanisms for external strain, which leading the graphene tend to crack at less than 5% strain. Although experiments and theoretical calculations show that the multilayer graphene can be stretched to 20–30% due to the crumbling structure and interplay between different graphene layers,[17,18] this performance is still insufficient to many applications conditions. Recently, several excellent works have demonstrated feasible stretchable graphene electrodes by designing various new structures, including graphene kirigami,[19] intercalating graphene scrolls,[20] entangled graphene mesh network,[21] crumpled graphene,[22] and conformal wrinkled structure,[23,24] etc. These novel structures confirmed the huge potential of graphene in the application of high-performance stretchable electrodes and devices. However, most of these materials require expensive high-quality chemical vapor deposition (CVD) graphene and a complicated etching process, which limited its large area scalable fabrication and damages the lattice; Second, the scalable fabrication technology could deposition and patterning the graphene film on the soft stretchable substrate is needed. Although, the photolithography,[19] pattern growth,[17] laser,[25] screen or ink-jet printing,[26] and shadow mask method[27] have been applied to patterning the graphene. These techniques often involve transferring, annealing, organic solvents, polymers additives, and surfactants during the operation process, which would negatively affect the optical and electrical performance of the graphene films. Furthermore, the soft elastomer polymer substrate is susceptible to damages from high-temperature annealing and organic solutions, thus these as mentioned techniques are not fully compatible with elastomer substrate. Thus, intrinsically stretchable strain-insensitive tactile sensor arrays based on the above graphene have yet to be demonstrated owing to the lack of scalable fabrication technology. Recently, we and other groups have developed a graphene interfacial self-assemble and transfer strategy, which could assemble graphene nanosheets on water surface into a film and could be further transferred to various flexible and stretchable substrates at mild atmosphere. This method has been used for the deposition of high-quality carbon nanofilms for the fabrication of various high-performance flexible devices, including sensors, and actuators. Xiao and co-workers[28,29] reported a strategy to scalable assemble CNTs on an air/water interface, which present potential applications in flexible electronics chemical sensors. Wang et al.[30] developed a programmable untethered soft robotics using air/water interface self-assembled graphene. The thickness of these films can be control in nanoscales. However, it is still hard to control the deposited film in a precise pattern way and regulating its stretchable performance, which further limits their application in high-precision and complex devices. In this respect, more attention should be paid in the designing of novel stretchable structure and developing new patterning technology in future works.

Herein, we described an elastomeric polymer induced conformal wrinkled graphene, the stretchable performance of which is highly tunable by regulating the wrinkle structure. The ultrathin graphene film was self-assembled by defect-free graphene nanosheets on the air–water interface and then transferred to Ar plasma treated poly(dimethylsiloxane) (PDMS) prestretched substrates. After the relief of strain, wrinkles are generated on the elastomeric substrates as the mismatched deformations between the inner layer and ultrathin silica-like layer on the surface due to plasma treatment. More importantly, combining with photolithography and shadow mask technique, we developed a fabrication process that enables the wafer-scale stretchable graphene film directly patterning on elastomer polymer substrate without high temperature, annealing, etching, or organic solvents operating. Based on this composite material, a semitransparent highly stretchable single-electrode triboelectric nanogenerator (SE-TENG) prepared, the TENG can be stretched to 100% strain without visible power output degradation. Furthermore, combining with the patterning techniques, intrinsically stretchable self-power tactile sensor arrays were fabricated, which presents a good application potential in human–machine interaction interfaces and strain-insensitive self-power pressure sensor arrays. Our work offers a possibility for the construction of a novel graphene-based fully stretchable soft electronic device, which can benefit from the desired high performance of graphene, including biocompatible, cost-effective, flexible, high conductivity, and stability.

2. Result and Discussion

The strategy for fabricating stretchable wrinkled Gr–PDMS composite is schematically illustrated in **Figure 1** and Figure S1 in the Supporting Information. First, the wrinkled PDMS substrate with desirable geometry was fabricated by the Ar plasma treatment method (Figure 1ai). As shown in Figure S1 in the Supporting Information, to precisely control the treatment area, a piece of photosensitive film was attached to the prestretched PDMS substrate, followed by lithography and developer solution treatment. Thus, a patterned mask was formed on the substrate. After the treatment of high-energy Ar plasma, the PDMS molecular chain near the surface without mask protection would crosslink together, which leading to the formation of a microscale denser crosslinked polymer thin

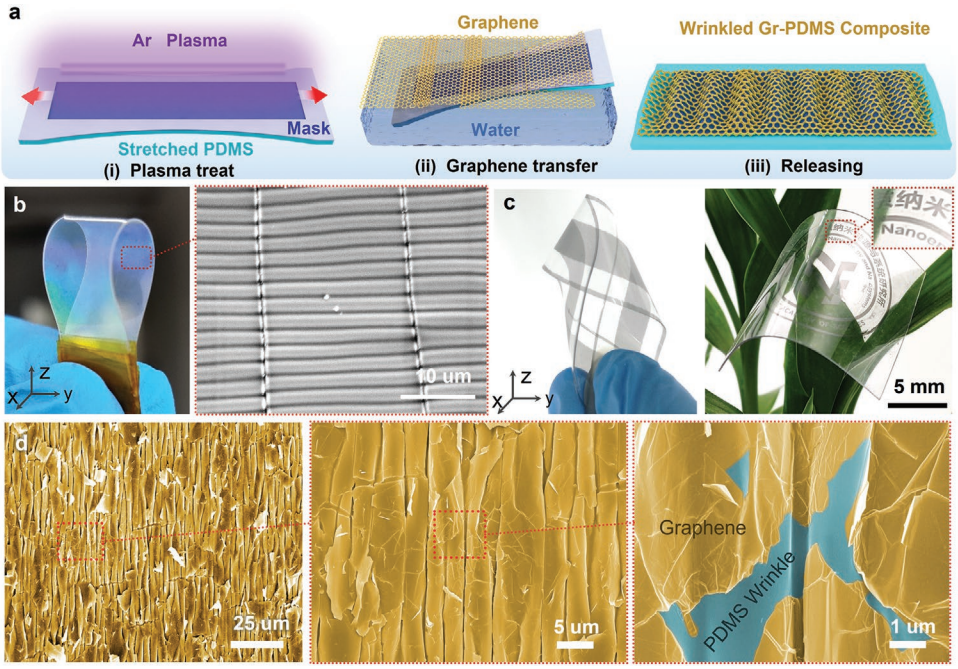

Figure 1. Fabrication of stretchable wrinkled Gr–PDMS composite. a) Schematic of the fabrication process of Gr–PDMS: i) The prestretched PDMS treated with Ar plasma under the protection of the patterned mask. ii) ISG film transferred to PDMS. iii) The graphene wrinkle formed after removing of mask and releasing it. b) Photographs and SEM images of wrinkled PDMS. c) Photographs of patterned Gr–PDMS composite. d) The SEM images of the wrinkle structure of Gr–PDMS composite.

layer on the surface (Figure S1aiv and Figure S1b, Supporting Information).[31] This high Young's modulus glass-like thin layer would induce wrinkle structure after releasing of strain (Figure S1 aiv and Figure S2, Supporting Information). The wrinkled structure can be well regulated by plasma treat time and prestretched quantity (ε) (Table S1, Supporting Information). As shown in Figure 1b, caused by the dispersion of light by sinusoidal fluctuated microtopography structure (Figure 1b right), a beautiful prismatic appearance of wrinkled PDMS can be observed (Figure 1b left). This wrinkled structure can induce the ultrathin graphene nanoflakes (Figure S3, Supporting Information), which were transferred and attached to the PDMS surface in the second step (Figure 1aii), to form the conformal graphene wrinkle structure. In this work, our previously reported interfacial self-assembled strategy was introduced for the preparation of the on-water graphene film. As the protection of the patterned mask, the semitransparent graphene film can precisely pattern deposition on PDMS substrate as we designed (Figure 1c). In the third step, after removing a mask and releasing it, the on-surface wrinkled graphene film can be formed (Figure 1aiii). As shown in Figure 1d and Figure S7 in the Supporting Information, the scanning electron microscope (SEM) images demonstrated that the graphene nanosheets strongly attach to the wrinkled PDMS surface. In comparison, without wrinkle structures, the graphene tends to locally detach from the surface and formed delaminated crumples (Figure S5, Supporting Information). On the one hand, the high Young's modulus skin structure is important for the mechanical robustness of wrinkled graphene since this thin layer is more resistant to crack formation.[24] On the other hand, the wrinkled graphene can unfold with the polymer wrinkle under strain instead of sliding apart from each other, thus the graphene nanosheets can maintain as an interconnected percolation network that enabled excellent conductivity under high strains.

The undulated microtopography of graphene induced by wrinkled PDMS enables excellent stretchability of wrinkled Gr–PDMS composite. The stretching mechanism of the wrinkled Gr–PDMS composite is schematically illustrated in **Figure 2**a. In the original state, the closely packed graphene sheets are strongly attached to the surface of wrinkled PDMS (Figure 2ai). Both the pristine and HNO_3-doped graphene films showed a high quality with little defect structure (H_2O treated $I_D/I_G = 0.76$, HNO_3 Doped $I_D/I_G = 0.85$) (Figure S6, Supporting Information) ratio. As shown in Figure S7 in the Supporting Information, HNO_3-treated graphene can be p-doped, leading to the high conductivity as the increase of charge carrier concentrations, thus the overlapping areas of stacked HNO_3-doped graphene sheets provide a better electrical transport pathway that contributes to the excellent conductivity. When the composite is under strain, the undulated graphene film extends with wrinkled PDMS. Since the preformed undulated structure contributes to the extension, overlapping areas of graphene sheets barely change. As shown in the SEM image (Figure 2aii), the stacked undulated structure of graphene film remains, only the amplitude decreases with applied strain. Hence the electrical transport pathway is preserved. When the composites are fully stretched, the graphene sheets are isolated by the gaps between graphene sheets induced by strain. The SEM image shows the graphene film is completely flattened (Figure 2aiii). Therefore, the electrical transport pathway is ruptured, and conductivity rapidly decreases. To demonstrate the potential of the Gr–PDMS composites in stretchable devices, we connected

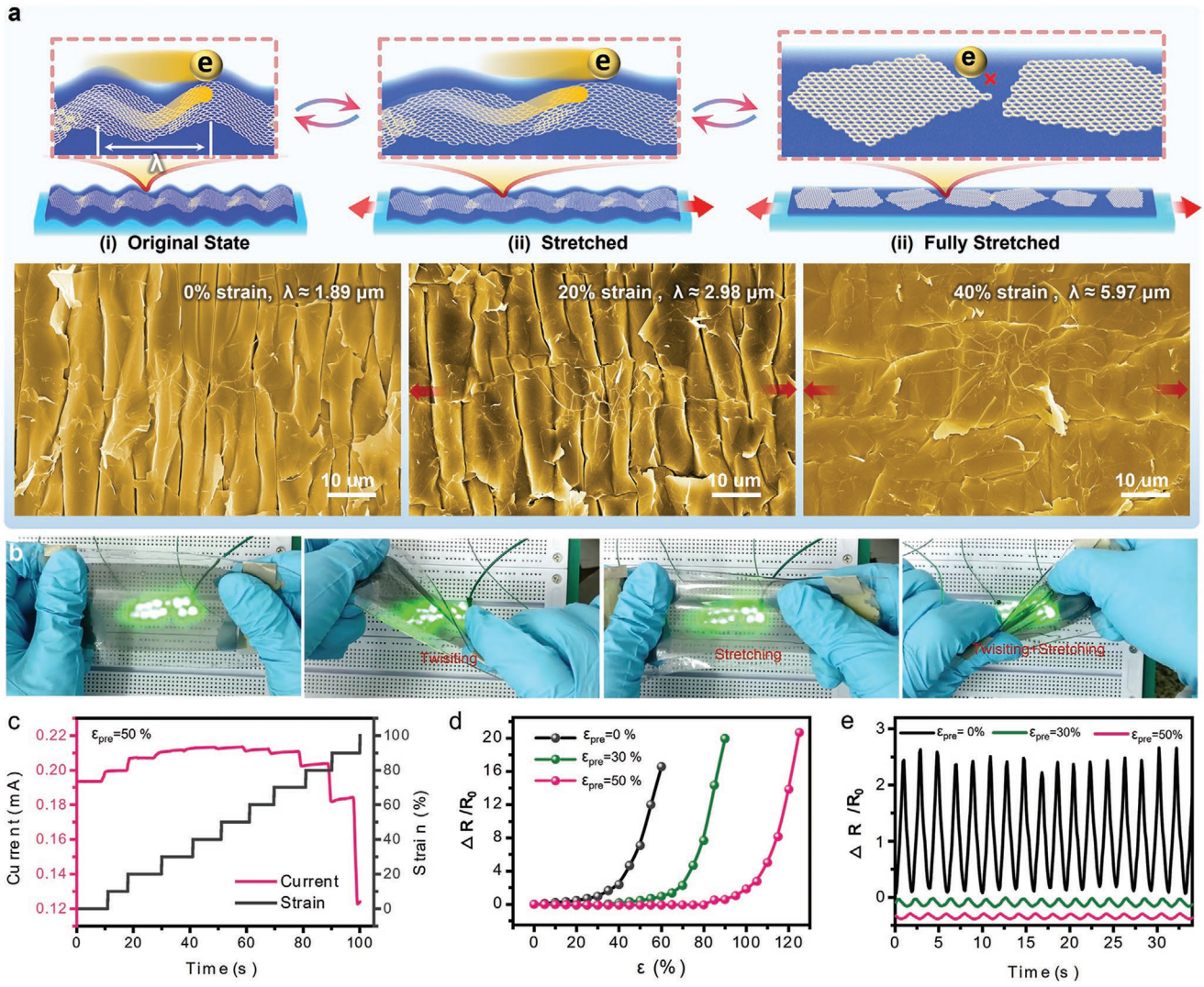

Figure 2. The stretchable mechanism and performance of wrinkled Gr–PDMS composite. a) Schematic and SEM of the Gr–PDMS composite under different strains. b) Photos of the Gr–PDMS composite conductor under normal state, twisting, stretching, and twisting while stretching. c) The current curve of Gr–PDMS composite conductor under different strains. The operating voltage is 1 V. d) Normalized resistance changes of different prestretched samples as a function of strain. e) Relative resistance changes of different Gr–PDMS composites were recorded for repeated stretching cycles with strains at 40%.

light-emitting diode (LED) lamps with the Gr–PDMS composites shown in Figure 2b. The light of LED lamps barely changes even when the composite was twisted, stretched, or twisting stretched, indicating its excellent stretchability.

The as-prepared wrinkled Gr–PDMS composite was characterized in terms of electrical stability under strains (Figure 2c). As the applied strain was changed in steps, the corresponding current presents three stages. During the first stage, when the applied strain varied from 0% to 30% a slight increase of current may be attributed to the closer stack of graphene sheets on concave areas and enlarged overlapping areas. During the second stage, when the applied strain varied from 30% to 80% the current slightly change. The compensation of undulated structure for the extension maintains the excellent conductivity of the wrinkled Gr–PDMS composite. In the final stage, when the applied strain varied from 80% to 100% the current rapidly decreases, caused by strain-induced isolation of graphene sheets. Therefore, our wrinkled Gr–PDMS composites possess excellent stretchability under a large strain range (from 0 to 80%), which may have wide application in stretchable electronics. To studying the effect of prestretch strain on the stretchability of Gr–PDMS composite, the Gr–PDMS composites prepared by different prestrain (0, 30%, and 50%) were compared. The Gr–PDMS composite prepared by larger prestrain possesses better stretchability. As shown in Figure 2d, the resistance change ratio ($\Delta R/R_0$) of the Gr–PDMS composites prepared by 50% prestrain barely change under 80% strain for stretching in the *x*-direction (the direction parallel to stretching direction). While, without wrinkle structure, the resistance change ratio in the *y*-direction (the direction orthogonal to stretching direction) (Figure S8, Supporting Information) only remains stable in a narrow range from 0% to 20%, which is

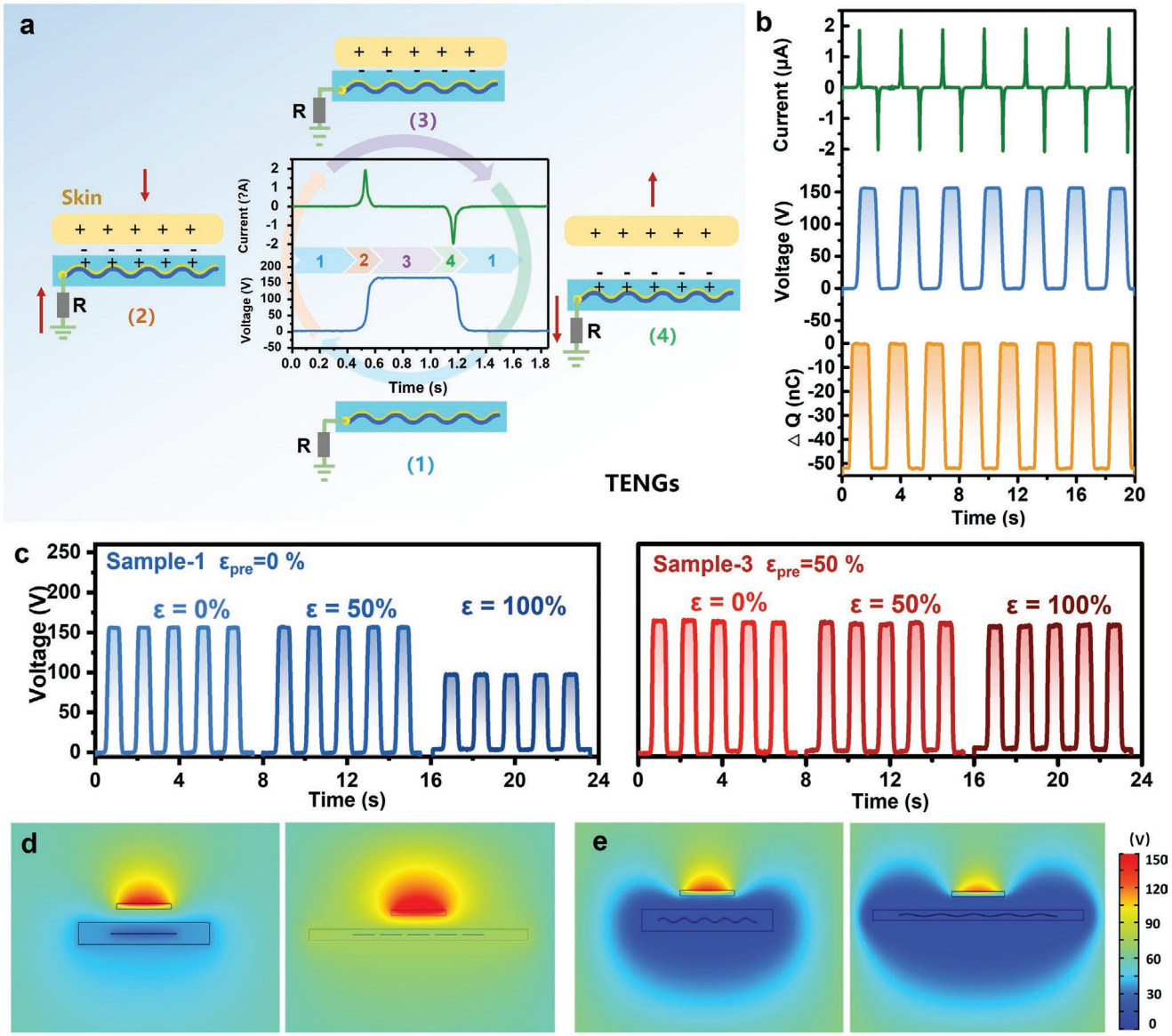

Figure 3. The working mechanical and performance of the wrinkled Gr–PDMS composite based SE-TENG. a) Schematic of the working principle of the graphene-based SE-TENG device. b) The current, output voltage, and charge signals during repeated touch cycles. c) The output voltage of sample 1 and sample 3 under different tensile strains. The simulation results of the charge distribution of the device without wrinkle structure d) and with wrinkle structure e) using the COMSOL software.

approximate to the performance of Gr–PDMS sample prepared by 0% prestrain. The repeated loading–unloading cycle experiments indicate the same results. The resistance changes the ratio of the Gr–PDMS composites prepared by 0 prestrain changes from 0 to 2.5, while the resistance changes ratio curve of the Gr–PDMS composites prepared by 30% prestrain and 50% prestrain exhibit much smaller fluctuation. In addition, the resistance changes ratio curve of the Gr–PDMS composites prepared by 50% prestrain is even more flattened than the resistance change ratio curve of the Gr–PDMS composites prepared by 30% prestrain. To investigate the long-time stability of the material, over 20 000 stretching cycles with strains at 100% were tested (Figure S9, Supporting Information). The result demonstrated that the conductivity performance of the composite is highly stable during long-time repeated stretching cycles.

For the application of graphene-PDMS composite, we prepared a flexible translucent SE-TENG. The triboelectric effects and electrostatic induction enable mechanical energy to be converted into electrical energy even on a flexible substrate. **Figure 3**a shows the schematic diagram of a single-electrode TENG device lighting LED. First, in the initial state (1), human skin and the PDMS friction layer of single-electrode TENG are separated, thus producing no charge. Second, when the skin gradually contacts the PDMS friction layer of TENG with the single electrode (2), due to electrostatic induction, the PDMS friction layer generates a negative charge, resulting in a positive charge of the skin. However, due to the triboelectric effects,

the undulated graphene layer carries a positive charge contrary to the triboelectric property of the PDMS friction layer, leading to the flow of electrons to the ground, and the LED is lighted. Then, when the skin is in full contact with the PDMS tribological layer (3), the two tribological layers are charged with positive and negative charges respectively due to the tribological effect. Finally, as the skin moves away from the SE-TENG, electrons flow from the ground to the SE-TENG device to light the LED due to electrostatic induction and tribological effects. Changes in positive and negative voltages (150 V) short-circuit current pulses (2 μA) and electric quantities (45 nC) during the entire operation were recorded (Figure 3b). As is shown in the diagram, the variation curves of voltage, current, and quantity are very stable within 20 s. In the whole working device, when the finger contacts the PDMS friction layer, the finger will be positively charged, while the PDMS friction layer will be negatively charged. Subsequently, electrons will flow to the ground, thus lighting the LED. As shown in Figure S10 in the Supporting Information, a total of 15 LEDs can be light up by our SE-TENG.

To evaluate the stretchability of devices, the whole working SE-TENG was stretched to measure the voltage variation under different stretching multiples (Figure 3f). The voltage of sample 1 (0% prestretched without wrinkle structure) did not change as much as the initial voltage value under the condition of 50% tension. However, as the device was stretched to 100%, the voltage decreased to about 98 V. In comparison, sample 3 (50% prestretched with wrinkle structure) showed nearly the same voltage value regardless of the tension was 50% or 100%, indicating its excellent stretchability. To understand the working principle of the devices, finite element analysis using COMSOL software was taken. As shown in Figure 3d, without the wrinkle structure, the graphene nanosheets would slide apart during the stretching process, thus the interconnect conducting network cracked, which leading to the decreasing of output voltage. In contrast, the concentrated stress in the graphene interconnect network can be dispersed by the unfurling of wrinkle structure, thus the conducting network can be maintained interconnected during a large stretching range. Figure 3e demonstrated that the output voltage values of the wrinkle structured device almost keep constant during a large stretch process (100%). Our SE-TENG based on graphene-PDMS composites has exhibited excellent stability during stretching, providing new possibilities for the development of stretching-insensitive graphene-based electronic products.

Owing to the excellent stretchability and conductivity, our triboiontronic sensor based on wrinkled Gr–PDMS composite can deform with human skin without performance degradation. Thus, we fabricated a triboiontronic sensor array that can be attached to human skin and capture the signals of figure contact. Then, we designed a human–machine interaction system based on our wrinkled Gr–PDMS composite sensor array. The system is composed of a triboiontronic sensor array based on wrinkled Gr–PDMS composite, signal acquisition, and remote transmitter circuit, and a computer (**Figure 4**a). The triboiontronic sensor array consists of nine triboiontronic sensors, which can distinguish the accurate position of the finger contact area. As shown in Figure 4b, the real-time triboiontronic signals of finger contact were captured by our triboiontronic sensor array. Subsequently, the triboiontronic signals were transformed into the positions of finger contacted area (Figure 4d), through corresponding sensors position (Figure 4c). Then, responses of the single sensor in different positions and the permutations of responses of multiple sensors were programmed to control the computer. As shown in Figure 4e, the soft device recognized the touch gesture and send complex machine instructions to the computer to open PowerPoint and print "Hello World" on screen.

The flexible pressure sensors have presented a great application potential in various fields, including real-time health monitoring, robot, and bionic hand, etc. Despite the high flexibility and performance, to accurately sense the pressure under the interference of dynamic mechanical deformation, including bending, twisting, and stretching, remains a great challenge. These deformations are inevitably induced large stress and strain in the sensor, thus leading to signal distortion. Hence, new concept materials and device that can perform stably on the curved and dynamic surface is needed. Herein, we prepared a high density and highly stretchable tactile sensor array 8 × 8 (area, 2.8 × 2.8 cm^2) based on our patterned wrinkled Gr–PDMS composite. As shown in **Figure 5**a, the extreme flexibility and stretchability of our tactile sensor array are demonstrated by poking the device with a sharp cross screwdriver. Our tactile sensor array was composed of the top PDMS layer working as electrification layer, column, and row graphene electrodes, the PDMS layer between electrodes working as insulator layer, and the bottom PDMS layer working as substrate (Figure 5b). The working mechanism of our wrinkled Gr–PDMS composite-based sensor is illustrated in Figure 5c. Our sensor is based on the single-electrode triboelectric nanogenerator. When human finger contacts top PDMS, the triboelectric charges are created because of the effect of contact electrification. Then, the negative charges on the PDMS layer induce positive charges in the graphene electrode, thus generating current from ground to graphene electrode. After the finger and PDMS are separated, the opposite current is generated. The responding output voltage signals of our sensors to applied pressure are shown in Figure 5d,e. The repetitive contact test under different pressure was carried out to depict the stability of our wrinkled Gr–PDMS composite-based sensor. As shown in Figure 5d, the voltage output of our wrinkled Gr–PDMS composite-based sensor merely changes under cyclic contact tests of different pressure. The responding voltage output of our wrinkled Gr–PDMS composite-based sensor to different applied pressure presents two linear response regions (region I from 0 to 2 kPa, region II from 2 to 10 kPa) shown in Figure 5e. It is worth to point that the response curve of the sensor at 0% and 50% strain shows a negligible change. As the output signal of each electrode is related to the intensity of pressure and its distribution, thus our self-power device presents a good application potential in the stretch-insensitive pressure sensing device. Figure 5f illustrates the application of our wrinkled Gr–PDMS composite-based sensor array in mimicking the human skin tactile sensation. To test the pressure intensity and distribution sensing ability of the device, we pressed two fingers with different pressure on the sensor array. The real-time tactile mapping data were acquired by a self-developed LabVIEW program.

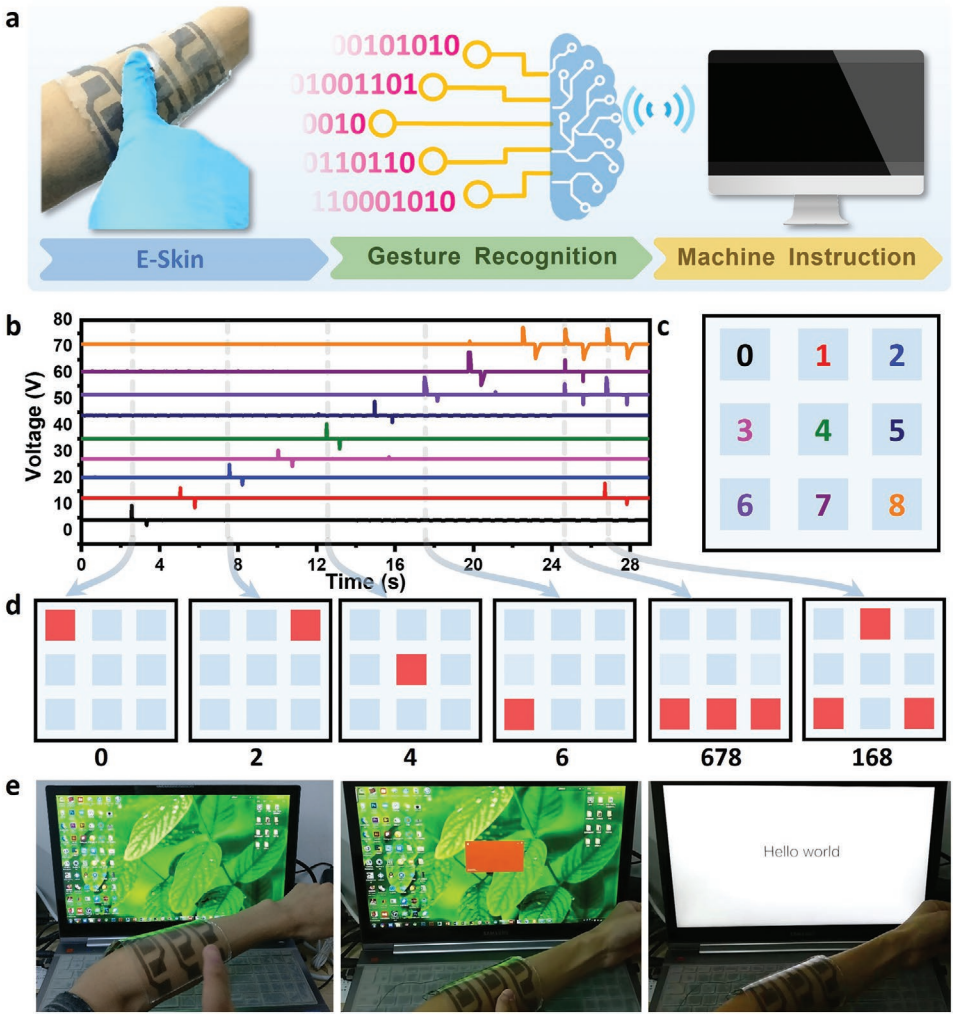

Figure 4. Design of the soft self-power tactile sensor arrays and their application in human–machine interaction. a) Schematic illustrations of the human–machine interaction system. b) Real-time multichannel voltage signals of the sensor arrays. The corresponding positions of different channel signals on the device. c) The corresponding trigger gesture at different times when fingers touch the device. e) Demo of the device act as soft-touch interfaces for computer control.

After data analysis and visualization, the pressure and position of finger contact are depicted in Figure 5g. The result demonstrated that the device accurately detected the finger's position and its pressure.

3. Conclusion

In conclusion, we presented an ultrathin stretchable and patternable wrinkled graphene composite material. In this paper, the conformal graphene wrinkles were induced by Ar plasma-treated PDMS prestretched substrates in a controllable manner. The crack-free topographical evolution of the wrinkled graphene film during the stretching process was observed, which demonstrated that the wrinkle structure accommodates the external mechanical stress in a normal state and disperse the stress by unfurling the structure to flat when stretched. This conformal wrinkled graphene structure can maintain its conductivity during a long strain range (0–100%), thus endow devices with high flexibility and stretchability. It is worth pointing out that our graphene films are self-assembled by graphene nanosheets on water, which can be easily transferred to soft polymer substrate free of harsh external conditions such as high-temperature annealing, etching, or organic solvents. Combining with lithography and shadow mask technique, the graphene can pattern on substrate precisely as we design, therefore the complicated stretchable device can be fabricated. In this work, a semitransparent and highly stretchable TENG and a self-powered E-skin device were fabricated. A 8 × 8 (area, 2.8 × 2.8 cm^2) intrinsically stretchable tactile sensor array was developed, which could sense the distribution and intensity of the applied pressure with negligible interference of large strain. These results proved that our novel composite material can proved a new opportunity for the construction of various new types of graphene-based or other 2D material strain-insensitive stretchable and wearable sensor arrays addressing challenging requirements such as stability, high conductivity, biocompatible, and cost-effective.

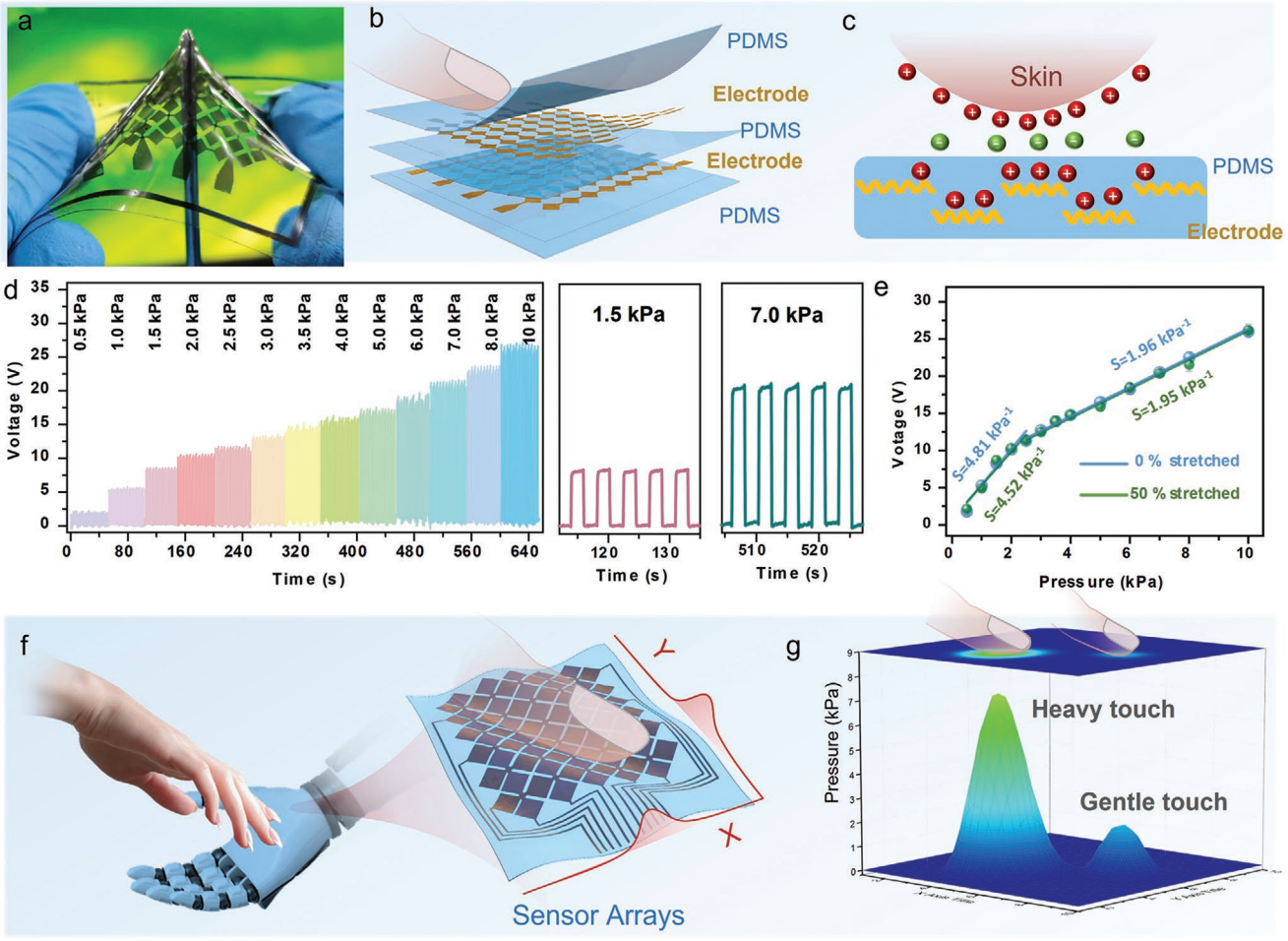

Figure 5. Highly flexible and intrinsically stretchable self-power sensor array as a core platform for pressure sensing skin electronics. a) An array of 8×8 (area, 2.8×2.8 cm^2) stretchable sensor under poking with a sharp cross screwdriver, showing its excellent flexibility. b) 3D diagram of the intrinsically stretchable self-power sensor array. c) The working principle of pressure sensing skin electronics. d) The output voltage signal of the sensor at 13 different pressures. e) The fitted pressure–voltage sensitivities curves of the sensor are under 0% and 50% strain. f) Demo of the device act as soft robot skin which could sense the distribution and g) intensity of the applied pressure.

4. Experimental Section

Reagents and Materials: PDMS (SYLGARD 184) was purchased from Dow Corning. Ag nanoflake (Silver flakes, 10 mum, ≥9.9% trace metals basis, 327077-10G), methyl isobutyl ketone, and nanoparticles were purchased from Sigma-Aldrich. The photoresist films were purchased from Shenzhen Kaishengyongheng Technology Co., Ltd. The Few-layer graphene is exfoliated from graphite through the solvent-assisted mechanical exfoliation method.[28]

Preparation of Wrinkled Gr–PDMS Composite: The interfacial self-assembled graphene (ISG) film is prepared through the Langmuir–Blodgett method. First, few-layer graphene was dispersed in anhydrous ethanol (0.5 mg mL^{-1}), followed by strong ultrasonication for 2 h to obtain uniform stable dispersion. The uniform graphene dispersion (≈200 mL m^{-2}) was then sprayed onto the water surface in a container, resulting in the formation of uniform graphene nanosheets self-assembled film floating on the liquid/air interface. Subsequently, microporous sponges were selected to carefully put on the water surface from the edge of the container to quickly siphon water from the system, followed by a visible decrease of the film area. The edge of the graphene film receded in the opposite direction of siphoning direction. Simultaneously, the graphene nanosheets were close packed. When the movement of the film stopped and further siphoning could not drive the film, the resultant homogeneous graphene film with a tightly packed structure was finally prepared.

The prepared PDMS films (Sylgard 184 Dow Corning) were first cut into strips with sizes of 5 cm × 1 cm. After being washed with water and anhydrous ethanol three times respectively and dried with Nitrogen, the PDMS strips were prestretched by different strains (0%, 10%, 30%, and 50%). Next, the photoresist films were attached to the PDMS strips, followed by exposing them to UV light (MA6 SUSS) through a designed mask for 15 s. Subsequently, the PDMS strips with patterned photosensitive films were obtained after treatment in developer solution for 5 min. Then, the prestretched PDMS strips were treated by Ar plasma (South Bay Tech., RIE 2000) at 100 W for different times (10, 20, and 30 min) under the protection of patterned photosensitive films. The ISG films were then transferred onto the PDMS strips. During the transferring process, the PDMS strips attached to plates were gradually inserted into the aqueous solution, followed by gradually lifting to pick up ISG films. Then the ISG-PDMS films were annealed by the hot wind for 10 min to improve the interface stability between ISG films and PDMS. After strain release, wrinkled Gr–PDMS composites were prepared.

Fabrication of the Devices: The PDMS films (Sylgard 184 Dow Corning) were first cut into squares with sides of 5 cm × 5 cm. After being washed with water and anhydrous ethanol three times respectively and dried

with nitrogen, the photosensitive films were attached to the PDMS squares. Then the PDMS squares with photoresist films were exposed to UV light for 15 s by using the UV photolithography technique (MA6 SUSS) through a designed mask. Subsequently, the PDMS squares with patterned photosensitive films were obtained after treatment in developer solution for 5 min. Next, the ISG films were transferred onto the PDMS squares with patterned photosensitive films. After the lift-off of the patterned photoresist film, the word line of graphene sensors was prepared. Then, PDMS (weight ratio of elastomer and crosslinker: 10:1, Sylgard 184 Dow Corning) was spin coated (500 rpm, 60 s) and cured at 70 °C for 2 h to encapsulate the graphene sensors. The preparation and encapsulation of bit lines of graphene sensors were prepared through the same procedure discussed above. Elastic conductive silver viscous ink was prepared by mixing Ag nanoflake, methyl isobutyl ketone, and silicon rubber (weight ratio 8:1:1). The ink was dipped between graphene and copper conductor to connect them.

Characterization: The micromorphology of the wrinkled PDMS and Gr–PDMS composite was characterized by the field-emission scanning electron microscope (SU8020 Hitachi). A high-impedance electrometer (Keithley 6514) was used to measure the current and resistant change of the wrinkled Gr–PDMS composite during the stretching process. The output voltage of the wrinkled Gr–PDMS composite-based triboiontronic sensors was also measured by the high-impedance electrometer (Keithley 6514). The contact pressure was measured by a pressure sensor (Nano17 Advanced Technology International). A digital multimeter (PXI-4072 National Instruments) with scanning matrix switches (PXI-2530, PXI-2630B, National Instruments) was employed to acquire output signals of the array device. A self-developed LabVIEW program was carried out to monitor the electrical signals of the array device.

Supporting Information

Supporting Information is available from the Wiley Online Library or from the author.

Acknowledgements

The authors thank the support of National Natural Science Foundation of China (Nos. 52003101, 52125205, U20A20166, 61675027, 61805015, and 61804011), Natural Science Foundation of Beijing Municipality (Z180011), China Postdoctoral Science Foundation (2020M673052 and 2021T140270), Shenzhen Science and Technology Program (Grant No. KQTD20170810105439418), and the Fundamental Research Funds for the Central Universities. Informed consent was obtained from the participant (J.H.) for their participation in the human experiments.

Conflict of Interest

The authors declare no conflict of interest.

Data Availability Statement

Research data are not shared.

Keywords

conformal wrinkles, graphene, self-powered, strain-insensitive sensors, tactile sensors

Received: July 27, 2021
Revised: October 19, 2021
Published online: December 10, 2021

[1] a) M. L. H. , C. Alex, B. C.-K. T. , J. B.-H. T. , B. Zhenan, *Adv. Mater.* **2013**, *25*, 5997; b) Y. Lee, J. Park, A. Choe, S. Cho, J. Kim, H. Ko, *Adv. Funct. Mater.* **2019**, *30*, 1904523; c) J. Tao, R. Bao, X. Wang, Y. Peng, J. Li, S. Fu, C. Pan, Z. L. Wang, *Adv. Funct. Mater.* **2018**, *29*, 1806379; d) J. C. Yang, J. Mun, S. Y. Kwon, S. Park, Z. Bao, S. Park, *Adv. Mater.* **2019**, *31*, 1904765; e) X. Wang, L. Dong, H. Zhang, R. Yu, C. Pan, Z. L. Wang, *Adv. Sci.* **2015**, *2*, 1500169; f) R. Bao, J. Tao, C. Pan, Z. L. Wang, *Small Sci.* **2021**, *1*, 2000060; g) C. Bauer, I. Veremchuk, C. Kunze, A. Benad, V. M. Dzhagan, D. Haubold, D. Pohl, G. Schierning, K. Nielsch, V. Lesnyak, A. Eychmüller, *Small Sci.* **2020**, *1*, 2000021; h) G. Yun, S.-Y. Tang, H. Lu, S. Zhang, M. D. Dickey, W. Li, *Small Sci.* **2021**, *1*, 2000080; i) Q. Guo, B. Huang, C. Lu, T. Zhou, G. Su, L. Jia, X. Zhang, *Mater. Horiz.* **2019**, *6*, 996; j) Y. Sun, T. Liu, Y. Kan, K. Gao, B. Tang, Y. Li, *Small Sci.* **2021**, *1*, 2100001; k) S. Yang, P. Qiu, L. Chen, X. Shi, *Small Sci.* **2021**, *1*, 2100005; l) J. Wu, H. Ma, P. Yin, Y. Ge, Y. Zhang, L. Li, H. Zhang, H. Lin, *Small Sci.* **2021**, *1*, 2000053.

[2] S. Chen, K. Jiang, Z. Lou, D. Chen, G. Shen, *Adv. Mater. Techol.* **2018**, *3*, 1700248.

[3] a) F. Li, J. Lu, Q. Zhang, D. Peng, Z. Yang, Q. Xu, C. Pan, A. Pan, T. Li, R. Wang, *Sci. Bull.* **2019**, *64*, 698; b) J. Liu, Z. Zhang, S. Qiao, G. Fu, S. Wang, C. Pan, *Sci. Bull.* **2020**, *65*, 477; c) Y. Liu, R. Bao, J. Tao, J. Li, M. Dong, C. Pan, *Sci. Bull.* **2020**, *65*, 70; d) C. Pan, L. Dong, G. Zhu, S. Niu, R. Yu, Q. Yang, Y. Liu, Z. L. Wang, *Nat. Photonics* **2013**, *7*, 752; e) C. Pan, J. Zhai, Z. L. Wang, *Chem. Rev.* **2019**, *119*, 9303; f) B. Wan, S. Guo, J. Sun, Y. Zhang, Y. Wang, C. Pan, J. Zhang, *Sci. Bull.* **2019**, *64*, 254; g) K. Xia, W. Wu, M. Zhu, X. Shen, Z. Yin, H. Wang, S. Li, M. Zhang, H. Wang, H. Lu, A. Pan, C. Pan, Y. Zhang, *Sci. Bull.* **2020**, *65*, 343.

[4] L.-B. Huang, X. Dai, Z. Sun, M.-C. Wong, S.-Y. Pang, J. Han, Q. Zheng, C.-H. Zhao, J. Kong, J. Hao, *Nano Energy* **2021**, *82*, 105724.

[5] L. Zhang, J. He, Y. Liao, X. Zeng, N. Qiu, Y. Liang, P. Xiao, T. Chen, *J. Mater. Chem. A* **2019**, *7*, 26631.

[6] a) X. Liu, G. Su, Q. Guo, C. Lu, T. Zhou, C. Zhou, X. Zhang, *Adv. Funct. Mater.* **2018**, *28*, 1706658; b) Y. Wang, X. Huang, X. Zhang, *Nat. Commun.* **2021**, *12*, 1291.

[7] Q. Hua, J. Sun, H. Liu, R. Bao, R. Yu, J. Zhai, C. Pan, Z. L. Wang, *Nat. Commun.* **2018**, *9*, 244.

[8] S. Wang, J. Xu, W. Wang, G.-J. N. Wang, R. Rastak, F. Molina-Lopez, J. W. Chung, S. Niu, V. R. Feig, J. Lopez, T. Lei, S.-K. Kwon, Y. Kim, A. M. Foudeh, A. Ehrlich, A. Gasperini, Y. Yun, B. Murmann, J. B. H. Tok, Z. Bao, *Nature* **2018**, *555*, 83.

[9] X. Wang, Y. Zhang, X. Zhang, Z. Huo, X. Li, M. Que, Z. Peng, H. Wang, C. Pan, *Adv. Mater.* **2018**, *30*, 1706738.

[10] Y. Zhang, Z. Huo, X. Wang, X. Han, W. Wu, B. Wan, H. Wang, J. Zhai, J. Tao, C. Pan, Z. L. Wang, *Nat. Commun.* **2020**, *11*, 5629.

[11] J. He, Y. Zhang, R. Zhou, L. Meng, T. Chen, W. Mai, C. Pan, *J. Materiomics* **2020**, *6*, 86.

[12] a) R. Hinchet, H.-J. Yoon, H. Ryu, M.-K. Kim, E.-K. Choi, D.-S. Kim, S.-W. Kim, *Science* **2019**, *365*, 491; b) H. Ouyang, Z. Liu, N. Li, B. Shi, Y. Zou, F. Xie, Y. Ma, Z. Li, H. Li, Q. Zheng, X. Qu, Y. Fan, Z. L. Wang, H. Zhang, Z. Li, *Nat. Commun.* **2019**, *10*, 1821.

[13] W. Fan, Q. He, K. Meng, X. Tan, Z. Zhou, G. Zhang, J. Yang, Z. L. Wang, *Sci. Adv.* **2020**, *6*, eaay2840.

[14] a) D. H. Ho, J. Han, J. Huang, Y. Y. Choi, S. Cheon, J. Sun, Y. Lei, G. S. Park, Z. L. Wang, Q. Sun, J. H. Cho, *Nano Energy* **2020**, *77*, 105262; b) Q. Xu, J. Wen, Y. Qin, *Nano Energy* **2021**, *86*, 106080; c) Z. Gao, S. Chen, R. Li, Z. Lou, W. Han, K. Jiang, F. Qu, G. Shen, *Nano Energy* **2021**, *86*, 106078; d) M. He, W. Du, Y. Feng, S. Li, W. Wang, X. Zhang, A. Yu, L. Wan, J. Zhai, *Nano Energy* **2021**, *86*, 106058; e) L.-B. Huang, J.-C. Han, S. Chen, Z. Sun, X. Dai, P. Ge, C.-H. Zhao, Q.-Q. Zheng, F.-C. Sun, J. Hao, *Nano Energy* **2021**, *84*, 105873.

[15] a) K. S. Novoselov, V. I. Fal'ko, L. Colombo, P. R. Gellert, M. G. Schwab, K. Kim, *Nature* **2012**, *490*, 192; b) Y. Zhu, S. Murali, W. Cai, X. Li, J. W. Suk, J. R. Potts, R. S. Ruoff, *Adv. Mater.* **2010**, *22*, 3906; c) Z. Komeily-Nia, L.-T. Qu, J.-L. Li, *Small Sci.* **2020**, *1*, 2000026; d) P. Majchrzak, R. Muzzio, A. J. H. Jones, D. Curcio, K. Volckaert, D. Biswas, J. Gobbo, S. Singh, J. T. Robinson, K. Watanabe, T. Taniguchi, T. K. Kim, C. Cacho, J. A. Miwa, P. Hofmann, J. Katoch, S. Ulstrup, *Small Sci.* **2021**, *1*, 2000075.

[16] a) J. He, P. Xiao, J. Shi, Y. Liang, W. Lu, Y. Chen, W. Wang, P. Théato, S.-W. Kuo, T. Chen, *Chem. Mater.* **2018**, *30*, 4343; b) J. He, P. Xiao, J. W. Zhang, Z. Z. Liu, W. Q. Wang, L. T. Qu, Q. Ouyang, X. F. Wang, Y. S. Chen, T. Chen, *Adv. Mater. Interfaces* **2016**, *3*, 1600169; c) P. Miao, J. Wang, C. Zhang, M. Sun, S. Cheng, H. Liu, *Nano-Micro Lett.* **2019**, *11*, 71; d) H. Liu, Q. Li, Y. Bu, N. Zhang, C. Wang, C. Pan, L. Mi, Z. Guo, C. Liu, C. Shen, *Nano Energy* **2019**, *66*, 104143; e) Z. Lou, S. Chen, L. Wang, K. Jiang, G. Shen, *Nano Energy* **2016**, *23*, 7.

[17] K. S. Kim, Y. Zhao, H. Jang, S. Y. Lee, J. M. Kim, K. S. Kim, J.-H. Ahn, P. Kim, J.-Y. Choi, B. H. Hong, *Nature* **2009**, *457*, 706.

[18] S. Won, Y. Hwangbo, S.-K. Lee, K.-S. Kim, K.-S. Kim, S.-M. Lee, H.-J. Lee, J.-H. Ahn, J.-H. Kim, S.-B. Lee, *Nanoscale* **2014**, *6*, 6057.

[19] M. K. Blees, A. W. Barnard, P. A. Rose, S. P. Roberts, K. L. McGill, P. Y. Huang, A. R. Ruyack, J. W. Kevek, B. Kobrin, D. A. Muller, P. L. McEuen, *Nature* **2015**, *524*, 204.

[20] N. Liu, A. Chortos, T. Lei, L. Jin, T. R. Kim, W. G. Bae, C. Zhu, S. Wang, R. Pfattner, X. Chen, R. Sinclair, Z. Bao, *Sci. Adv.* **2017**, *3*, 1700159.

[21] J. Han, J.-Y. Lee, J. Lee, J.-S. Yeo, *Adv. Mater.* **2018**, *30*, 1704626.

[22] J. Zang, S. Ryu, N. Pugno, Q. Wang, Q. Tu, M. J. Buehler, X. Zhao, *Nat. Mater.* **2013**, *12*, 321.

[23] K. M. Hu, Y. Q. Liu, L. W. Zhou, Z. Y. Xue, B. Peng, H. Yan, Z. F. Di, X. S. Jiang, G. Meng, W. M. Zhang, *Adv. Funct. Mater.* **2020**, *30*, 2003273.

[24] D. Rhee, J. T. Paci, S. Deng, W.-K. Lee, G. C. Schatz, T. W. Odom, *ACS Nano* **2020**, *14*, 166.

[25] Y. Ling, W. Pang, X. Li, S. Goswami, Z. Xu, D. Stroman, Y. Liu, Q. Fei, Y. Xu, G. Zhao, B. Sun, J. Xie, G. Huang, Y. Zhang, Z. Yan, *Adv. Mater.* **2020**, *32*, 1908475.

[26] a) W. J. Hyun, E. B. Secor, M. C. Hersam, C. D. Frisbie, L. F. Francis, *Adv. Mater.* **2015**, *27*, 109; b) J. Li, F. Ye, S. Vaziri, M. Muhammed, M. C. Lemme, M. Ostling, *Adv. Mater.* **2013**, *25*, 3985; c) E. B. Secor, S. Lim, H. Zhang, C. D. Frisbie, L. F. Francis, M. C. Hersam, *Adv. Mater.* **2014**, *26*, 4533.

[27] Z. Chen, T. Ming, M. M. Goulamaly, H. M. Yao, D. Nezich, M. Hempel, M. Hofmann, J. Kong, *Adv. Funct. Mater.* **2016**, *26*, 5061.

[28] J. He, P. Xiao, W. Lu, J. Shi, L. Zhang, Y. Liang, C. Pan, S.-W. Kuo, T. Chen, *Nano Energy* **2019**, *59*, 422.

[29] a) P. Xiao, Y. Liang, J. He, L. Zhang, S. Wang, J. Gu, J. Zhang, Y. Huang, S.-W. Kuo, T. Chen, *ACS Nano* **2019**, *13*, 4368; b) Y. Wang, L. Wang, T. Yang, X. Li, X. Zang, M. Zhu, K. Wang, D. Wu, H. Zhu, *Adv. Funct. Mater.* **2014**, *24*, 4666.

[30] S. Wang, Y. Gao, A. Wei, P. Xiao, Y. Liang, W. Lu, C. Chen, C. Zhang, G. Yang, H. Yao, T. Chen, *Nat. Commun.* **2020**, *11*, 4359.

[31] C. Hanske, M. Tebbe, C. Kuttner, V. Bieber, V. V. Tsukruk, M. Chanana, T. A. F. König, A. Fery, *Nano Lett.* **2014**, *14*, 6863.